ROYAL SOCIETY
OF CHEMISTRY

Check for updates

Aqueous (co)polymer stabilisers for size-controlled 2–5 nm gold nanoparticle synthesis with tuneable catalytic activity†

Daniel J. Traynor, [ID] [a] Elena Ureña-Horno, [ID] [a] James J. Hobson, [ID] [ab] Elliot J. Croft, [ID] [a] Stephanie E. Edwards, [ID] [a] Steve P. Rannard [ID] [ab] and Marco Giardiello [ID] *[a]

Gold nanoparticles, or colloidal gold (AuNP), represent one of the most significant and established forms of sub-micron inorganic structures to be researched in recent years. AuNP physical and chemical properties are dictated by both their ligand surface chemistry and their size, which can be manipulated and tuned during their synthesis. In this study, aqueous linear and branched homo-polymers and (co)polymers are developed and used as surface stabilisers during AuNP synthesis. A library of such polymeric stabilisers were prepared using conventional free radical polymerisation techniques to incorporate units of varying AuNP surface binding affinity, using methacrylic acid (MAA) and oligo (ethylene glycol) methyl ether methacrylate (OEGMA) monomers and dodecane thiol (DDT) as the chain transfer agent. AuNPs were synthesised *via* $HAuCl_4 \cdot 3H_2O$ reduction in the presence of the prepared library of polymeric stabilisers. It was observed that variation of (co)polymer composition and architecture allowed for size-controlled gold nanoparticle synthesis, with AuNPs prepared ranging from 2.17 ± 0.07 nm to 4.83 ± 0.04 nm as determined by UV-vis spectroscopy. Varying (co)polymer composition and architecture also yielded variable catalytic behaviour in the reduction of 4-nitrophenol (4-NP) to 4-aminophenol (4-AP) using $NaBH_4$, with catalytic reaction rates ranging from 1.0 s^{-1} to 45.3 s^{-1} and induction times ranging from 0 seconds to 2070 seconds depending on the polymeric stabilisers employed during synthesis.

Introduction

Gold nanoparticles (AuNP), often referred to as colloidal gold, are one of the most established forms of metal nanoparticles due to their broad range of applications and their distinctive size dependent optical properties.[1–4] In medicine, colloidal gold has been researched for a wide number of both diagnostic and therapeutic applications, for example as optical biosensors for disease detection,[5–9] targeted drug delivery systems,[10,11] photothermal therapy,[12,13] gene therapy,[14,15] and radiotherapy.[16–18] Outside of medicine, AuNPs have been employed as printable inks for electronic devices,[19,20] in fuel cell applications,[21] and as catalysts for a number of chemical reactions.[22–25] A particularly well known use for AuNP catalysts is the reduction of

4-nitrophenol (4-NP) to 4-aminophenol (4-AP) using sodium borohydride ($NaBH_4$) as the reducing agent, which was explored herein.[26–29]

AuNPs vary in both size (*i.e.* approximately 1 nm to 100 nm) and shape (*e.g.* spheres, rods, cubes, stars). The structural variability arises from the methodology that is employed during their synthesis.[30] AuNPs are typically prepared by reduction of chloroauric acid (gold(III) chloride trihydrate ($HAuCl_4 \cdot 3H_2O$)) in the presence of surface stabilising ligands to prevent particle aggregation. Upon Au(III) reduction, gold atoms begin to precipitate and aggregate to form nanoscale particles upon which the stabilisers bind during growth, with vigorous mixing of the solution required to ensure particle formation is uniform in size. One of the most common synthetic methods is the Turkevich–Frens method in which sodium citrate is employed as both the reducing agent and as a surface stabiliser.[31,32] Another common method is the Brust–Schiffrin method, which employs sodium borohydride ($NaBH_4$) as the reducing agent used in the presence of thiol containing stabilising molecules;[33–35] AuNP surfaces have a particularly high affinity for thiol groups as well as an affinity for hydroxyl and carboxylic

[a] *Department of Chemistry, University of Liverpool, Crown Street, Liverpool L69 7ZD, UK. E-mail: marco.giardiello@liverpool.ac.uk*

[b] *Centre of Excellence for Long-acting Therapeutics, University of Liverpool, West Derby Street, Liverpool L7 8TX, UK*

† Electronic supplementary information (ESI) available: ^{1}H NMR data; UV-vis absorption data for AuNP salt stability and catalytic studies. See DOI: https://doi.org/10.1039/d2nj03257k

This journal is © The Royal Society of Chemistry and the Centre National de la Recherche Scientifique 2022

acid groups.[36,37] The surface structure and the binding nature of such ligands coupled with the synthetic conditions employed can dictate AuNP sizes produced during synthesis as well as the surface chemistry and AuNP stability.[38–40] A number of research groups have studied the use of functionalised polymers as stabilising ligands for size controlled AuNP synthesis,[41,42] such as thiol and thioether functionalised polyethylene glycol (PEG),[43–45] poly(acrylic acid) (PAA) and poly(methacrylic acid) (PMAA).[46,47]

The aim of the current study was to generate a range of water-soluble (co)polymers to act as AuNP surface stabilisers, each prepared with varied degrees of affinity for AuNP surface binding. The (co)polymers were employed in a simple one step synthetic method for AuNP formation through the reduction of chloroauric acid by $NaBH_4$, mimicking already published routes.[47] Herein, a library of both linear and branched homo-polymers and (co)polymers were prepared, incorporating the monomer units methacrylic acid (MAA) and oligo (ethylene glycol) methyl ether methacrylate (OEGMA) via free radical polymerisation using dodecane thiol (DDT) as the chain transfer agent (CTA). An analogous homo-polymer was also synthesised using Atom Transfer Radical Polymerisation (ATRP) to study the impact of the thioether that is a consequence of the use of DDT as a CTA under conventional free radical conditions (Fig. 1). Thus, each polymeric structure contains functional groups with varied affinity for AuNP surface binding in differing ratios:[36,37] strong affinity for thioether from the DDT residue; comparably moderate affinity for carboxylic acid groups from MAA residues; comparatively minimal affinity for ether groups from polyethylene glycol (PEG) chains of OEGMA residues. The investigative aims were twofold: (1) a synthetic aim to explore the effect of variability in polymeric composition, architecture, and concentration on controlled particle size when used as surface stabilisers during AuNP synthesis; (2) a surface chemistry aim to investigate the influence of polymeric stabiliser effects on AuNP catalytic activity, conducted by monitoring the variability in the rate of catalytic reduction of 4-NP to 4-AP by $NaBH_4$.

Fig. 1 Chemical structures of homo-polymers and (co)polymers generated. Each were prepared targeting DP_n = 50, with $x : y$ values at 0 : 50; 2.5 : 47.5; 5 : 45; 7.5 : 42.5; 10 : 40.

Materials and methods

Materials

Methacrylic acid >99% (MAA), oligo(ethylene glycol)methyl ether methacrylate (average M_n 300) (OEGMA), ethylene glycol dimethacrylate >98% (EGDMA), dodecane thiol >98% (DDT), 1-dodecanol, triethylamine (TEA), α-bromoisobutyl bromide, azobisisobutyronitrile >98% (AIBN), gold(III) chloride trihydrate >99.9% ($HAuCl_4 \cdot 3H_2O$)), sodium borohydride >98% ($NaBH_4$), 4-nitrophenol >99% (4-NP), Cu(I)Cl >99%, 2,2′-bipyridyl >99% (bipy), aluminium oxide (activated, basic), Dowex Marathon exchange resin, Amberlyst resin, methanol (HPLC grade), ethanol (HPLC grade) and tetrahydrofuran (THF) (HPLC grade) were all purchased from Sigma-Aldrich and used without any further preparation. $CDCl_3$ NMR solvent was purchased from GOSS Scientific.
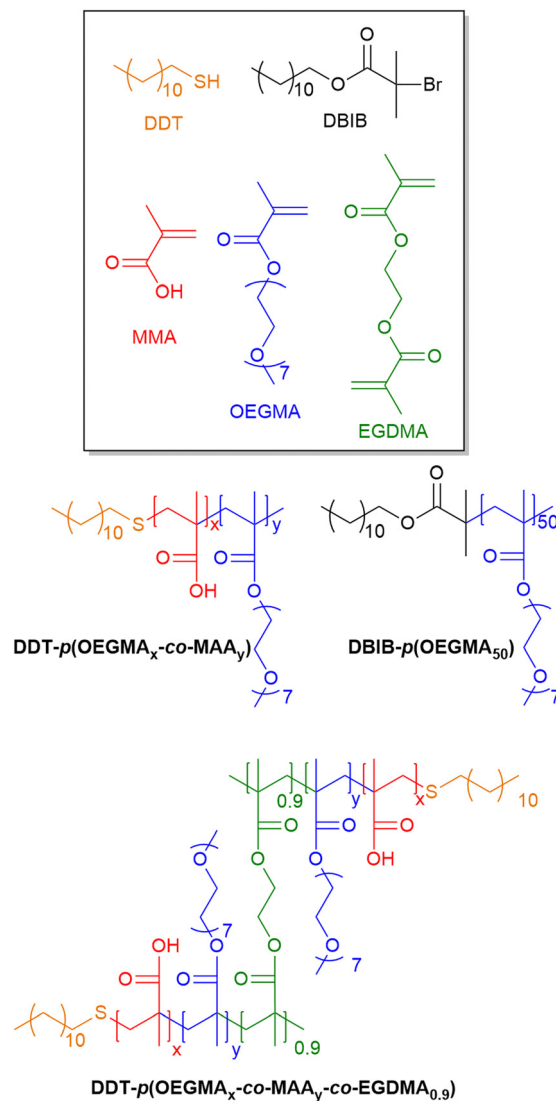
Equipment

^{1}H NMR spectroscopy: ^{1}H NMR spectra were recorded in $CDCl_3$ using a 400 MHz Brüker Avance spectrometer. Chemical shifts (δ) are reported in parts per million (ppm) with respect to an internal reference of tetramethylsilane (TMS). Triple detection size exclusion chromatography: TD-SEC was performed using a Malvern Viscotek instrument equipped with a GPCmax VE2001 auto-sampler, two Viscotek T6000 columns (and a guard column), a refractive index (RI) detector VE3580 and a 270 Dual Detector (light scattering and viscometer) with a mobile phase of THF containing 2 v/v% of triethylamine and a flow-rate of 1 mL min^{-1}. Dynamic light scattering: DLS studies were performed using a Malvern Zetasizer Nano ZS equipped with a 4 mW He–Ne, 633 nm at a temperature of 25 °C and using 1 cm plastic disposable cuvettes for aqueous dispersions. Malvern Zetasizer software version 7.13 was used for data analysis using the instruments automatic optimisation settings. Zeta potential: measurement of

zeta potential (ζ) also used the Malvern Zetasizer Nano ZS and were carried out at 25 °C; measurements were obtained using the instruments automatic optimisation settings. Ultraviolet-visible spectrophotometry: UV-vis absorption was recorded using a Thermo Scientific NanoDrop 2000c spectrometer operating in cuvette mode. Measurements were taken in triplicate, from which the average was used for error calculation. Transmission electron microscopy: TEM characterisation was carried out using a FEI 120 kV Tecnai G2 Spirit BioTWIN. TEM grids were prepared as follows; 10 μl of the particle dispersions were pipetted directly onto carbon films on 300 mesh TEM grids (Agar Scientific) and allowed to dry for 24 hours. Particle size distribution was analysed using ImageJ software measuring over 100 AuNPs for the statistical analysis. Note: DLS, zeta potential, UV-vis and TEM measurements were taken directly from the nanoparticle dispersions following synthesis without any additional filtration, centrifugation or dilution. The approximate pH of all samples were measured to be pH 8.

Synthesis of linear DDT-p(OEGMA$_x$-co-MAA$_y$) and branched DDT-p(OEGMA$_x$-co-MAA$_y$-co-EGDMA$_{0.9}$) by free radical polymerisation

For the free radical synthesis of both linear DDT-p(OEGMA$_x$-co-MAA$_y$) and branched linear DDT-p(OEGMA$_x$-co-MAAy-co-EGDMA$_{0.9}$), a target DP$_n$ = 50 monomer units was prepared using varied ratios of the MMA : OEGMA always towards a final 16.7 mmols of the combined monomers. For linear (co)polymers, MAA and OEGMA were added together to a 25 mL round-bottom flask, fitted with a stirrer bar in the following MAA : OEGMA proportions: DDT-p(OEGMA$_{50}$) = 0 g MAA : 5 g OEGMA (0 : 16.7 mmol); DDT-p(OEGMA$_{47.5}$-co-MAA$_{2.5}$) = 0.07 g MAA : 4.76 g OEGMA (0.84 : 15.87 mmol); DDT-p(OEGMA$_{45}$-co-MAA$_5$) = 0.14 g MAA : 4.51 g OEGMA (1.67 : 15.03 mmol); DDT-p(OEGMA$_{42.5}$-co-MAA$_{7.5}$) = 0.22 g MAA : 4.26 g OEGMA (2.51 : 14.2 mmol); DDT-p(OEGMA$_{40}$-co-MAA$_{10}$) = 0.29 g MAA : 4.01 g OEGMA (3.34 : 13.36 mmol). For branched (co)polymers, EGDMA (0.066 g, 0.334 mmol) was added to reaction mixture with the MMA : OEGMA mixtures the same proportions as for the linear, with polymerisation conditions conducted in the identical manner. DDT (0.068 g, 0.334 mmol) and AIBN (0.041 g, 0.251 mmol) were then added followed by ethanol (HPLC grade; 50 v/v% based on OEGMA). The solutions were degassed with an N$_2$ purge for approx. 15 minutes whilst stirring. After initiation, the N$_2$ flow was removed and the flasks rendered air-tight with parafilm. The solutions were heated to 70 °C and left for 24 hours. After approx. >99% conversion (judged by ^{1}H NMR analysis) crude materials were left to cool to terminate the polymerisations. The crudes were added dropwise through a syringe into cold PET ether allowing for precipitation of the polymeric materials, which were isolated via filtration. Samples were dried using a spiral dryer to remove any excess solvent, before being placed in a vacuum oven overnight to yield the polymeric materials as brown viscous oils.

Synthesis of 2-dodecyl 2-bromoisobutyrate (DBiB)

Following literature methods,[48] 1-dodecanol (9.32 g, 50.0 mmol, 1.00 equiv.) and TEA (6.07 g, 60.0 mmol, 1.20 equiv.) were dissolved in dichloromethane (DCM, 70 mL). A solution of α-bromoisobutyl bromide (13.8 g, 60.0 mmol, 1.20 equiv.) in DCM was added dropwise to the mixture via a pressure equalising dropping funnel and stirred in an ice bath under an N$_2$ atmosphere. After addition, the reaction vessel was left to warm to ambient temperature and was left stirring for 24 hours. The solution was washed with NaHCO$_3$ (1 M, 1 × 50 mL) and deionised water (4 × 50 mL). The organic layer was then dried over anhydrous MgSO$_4$, filtered, and concentrated in vacuo. The product was then passed through a basic alumina column. The product was isolated as a clear oil in 53% yield (8.91 g) and the correct structure was confirmed using ^{1}H and ^{13}C NMR spectroscopy. ^{1}H NMR (400 MHz, CDCl$_3$) δ (ppm) = 0.81 (t, J = 6.6 Hz, 3H), 1.19 (m, 18H), 1.61 (m, 2H), 1.86 (s, 6H, CH$_3$), 4.08 (t, J = 6.6 Hz, 2H). ^{13}C NMR (100 MHz, CDCl$_3$) δ (ppm) = 14.1, 22.7, 25.8, 28.4, 29–30, 32.0, 56.0, 66.2, 171.8.

Synthesis of DBIB-p(OEGMA)$_{50}$ by ATRP

For the ATRP synthesis of linear DBIB-p(OEGMA)$_{50}$ with a target DP$_n$ = 50 monomer units, OEGMA (5 g, 16.7 mmol) and DBIB (0.112 g, 0.334 mmol) were added to a 25 mL round-bottom flask fitted with a magnetic stirrer bar. Methanol (HPLC grade; 50 v/v% based on OEGMA) was added and the solution was degassed with an N$_2$ purge for approx. 15 minutes whilst stirring. Cu(I)Cl (0.033 g, 0.334 mmol) and bipy (0.104 g, 0.668 mmol) were weighed together and quickly added to the stirring solution whilst maintaining a positive nitrogen flow. After initiation, the N$_2$ flow was removed and the flask was rendered air-tight with parafilm. The solution was left to polymerise at ambient temperature. After approx. >99% conversion (judged by ^{1}H NMR analysis) the reaction was exposed to the atmosphere and manually terminated via addition of THF (approx. 200 mL). Once fully terminated, Dowex Marathon exchange beads (~10 g) were added to the solution and stirred for approx. 20 minutes, to aid catalyst removal. The beads were removed by filtration and the remaining solution was passed over a basic alumina column to remove residual catalyst/ligand complex. The mixture was concentrated under vacuum to remove the majority of THF, followed by precipitation of the viscous solution into cold hexane. The solution was then filtered to yield the polymer material as a white powder.

Gold nanoparticle (AuNP) synthesis

Aqueous stock solutions of each homo-polymer and (co)polymer were prepared by dissolving 175 mg of each in 5 mL distilled water (35 mg mL^{-1}) and left to stir overnight to aid dissolution. Separately, a stock solution of gold(III) chloride trihydrate was prepared by dissolving 39.38 mg of HAuCl$_4$·3H$_2$O in 19 mL of distilled water (5.26 mM). Reaction solutions were prepared by addition of 1.9 mL of the HAuCl$_4$·3H$_2$O stock solution to 2 mL, 1 mL or 0.5 mL of polymeric stock solutions (thus 70 mg, 35 mg and 17.5 mg homo-polymer or (co)polymer respectively). Further distilled water was added to adjust the total final volume of each solution to 20 mL. Thus, the final solution concentration of HAuCl$_4$·3H$_2$O was 0.5 mM. Each solution was stirred vigorously for 60 minutes to complete

dissolution. 2 mL of aqueous $NaBH_4$ (50 mM) was added rapidly in two 1 mL aliquots to each solution, resulting in a sudden colour change from a pale-yellow solution to a deep red solution. The reaction vessels were then sealed and left to rapidly and uniformly stir overnight. Reaction mixtures were subsequently analysed as prepared *via* UV-vis spectroscopy, observing the absorption ratios of the surface plasmon band (A_{spr}) at around 520 nm with the absorpsion at 450 nm (A_{450}) to determine AuNP size following literature methods.[49]

AuNP salt stability studies

A 1 M aqueous stock solution of NaCl was prepared. The solution was added to 1 mL of each AuNP dispersion in 200 mL aliquots; each 200 mL addition was therefore approx. 11 mg NaCl. After each addition, the AuNP dispersion was monitored by UV-vis spectroscopy, observing the absorption ratios of the surface plasmon band (A_{spr}) at around 520 nm with the absorpsion at 450 nm (A_{450}) to observe any change in AuNP. A total of six 200 mL NaCl additions were made per AuNP sample, giving a final NaCl concentration of 0.55 M.

Catalytic reduction of 4-nitrophenol (4-NP) to 4-aminophenol (4-AP) studies

A 1 mM aqueous stock solution of 4-nitrophenol (4-NP) was prepared; this stock solution was used consistently for all catalysis experiments. For each reaction, 20 μL of the 4-NP stock solution were added to 980 μL of distilled water. Subsequently, 2 mL of 0.5 mg mL^{-1} $NaBH_4$ solution were added and the time = 0 UV-vis absorption was immediately measured, observing the intensity of the 4-NP absorption band at ~400 nm. Separately, 25 μL of each of the prepared AuNP mixtures were added in turn to another UV-vis cuvette, which was then placed in the UV-vis spectrometer. Catalytic reactions were initiated by addition of 1 mL of the 4-NP/$NaBH_4$ solution to the AuNP mixture cuvette; thus reactions were conducted directly in the UV-vis spectrometer and immediately analysed, monitoring the reduction of the 4-NP absorption band at regular time intervals as the catalytic reaction progressed.

Results and discussion

Linear and branched homo-polymer and (co)polymer synthesis

A library of both linear and branched (co)polymers were synthesised, with the synthetic strategy of increasing AuNP surface affinity (Fig. 1). The target DP_n was fixed at 50 monomer units, thus to a mixture of DDT and azobisisobutyronitrile (AIBN), combinations of the monomers MAA and OEGMA were added together in the following MAA:OEGMA proportions: 0:50; 2.5:47.5; 5:45; 7.5:42.5; 10:40 to generate the homo-polymer and (co)polymers outlined in Table 1, with the molecular weight distributions for each determined by Triple Detection Size Exclusion Chromatography (TD-SEC). It was theorised that the progressive substitution of carboxylic acid bearing MAA for OEGMA would generate polymeric stabilisers with an increasing affinity for AuNP surfaces as more MAA is incorporated. Branched (co)polymers were generated in an identical manner, however 0.9 equivalents (*cf.* DDT) of ethylene glycol dimethacrylate (EGDMA) were added. In order to observe the effect of the presence of the thioether on AuNP surface binding, one further linear homo-polymer, DBIB-p(OEGMA$_{50}$), was prepared incorporating dodecyl 2-bromoisobutyrate (DBIB) in place of DDT; ATRP was employed in this instance due to the inability for the initiator group to undergo free radical polymerisation. High conversion was confirmed by ^1H NMR, which indicates the loss of vinyl monomer peaks at around 6.15 and 5.60 ppm, with >97% conversion confirmed across all homo-polymers and (co)polymers (see Fig. S1–S11, ESI†). ^1H NMR was also used to confirm the (co)monomer composition through the ratio of integrations of the chemical shift resonances for the terminal methyl groups of OEGMA at 3.38 ppm with the combined peak for the MAA and OEGMA methyl groups present in the polymeric backbones at 0.85–1.0 ppm. ^1H NMR confirmed the ratio to match the expected MAA incorporation across all homo-polymers and (co)polymers.

Size controlled gold nanoparticle (AuNP) synthesis

AuNPs were synthesised by reduction of $HAuCl_4 \cdot 3H_2O$ by $NaBH_4$ with each homo-polymer and (co)polymer present at three different concentrations with respect to Au(III). Aqueous stock solutions of each polymeric material were prepared at 35 mg mL^{-1} at pH 8, while separately, a 5.26 mM aqueous stock solution of $HAuCl_4 \cdot 3H_2O$ was also prepared. To a series of fixed

Table 1 Summary of composition, predicted AuNP surface binding affinity, and TD-SEC analysis of the linear and branched (co)polymer library generated for this study

(Co)polymer structure	OEGMA %	MAA %	$M_n{}^a$ (g mol^{-1})	$M_w{}^a$ (g mol^{-1})	Đ^a
DDT-p(OEGMA$_{50}$)	100	0	14 542	27 956	1.922
DDT-p(OEGMA$_{47.5}$-co-MAA$_{2.5}$)	95	5	17 629	29 767	1.688
DDT-p(OEGMA$_{45}$-co-MAA$_5$)	90	10	17 062	27 406	1.606
DDT-p(OEGMA$_{42.5}$-co-MAA$_{7.5}$)	85	15	29 178	39 983	1.370
DDT-p(OEGMA$_{40}$-co-MAA$_{10}$)	80	20	38 211	52 864	1.383
DDT-p(OEGMA$_{50}$-co-EGDMA$_{0.8}$)	100	0	14 830	95 963	6.471
DDT-p(OEGMA$_{47.5}$-co-MAA$_{2.5}$-co-EGDMA$_{0.9}$)	95	5	15 748	185 290	11.766
DDT-p(OEGMA$_{45}$-co-MAA$_5$-co-EGDMA$_{0.9}$)	90	10	19 744	85 971	4.354
DDT-p(OEGMA$_{42.5}$-co-MAA$_{7.5}$-co-EGDMA$_{0.9}$)	85	15	18 472	117 804	6.377
DDT-p(OEGMA$_{40}$-co-MAA$_{10}$-co-EGDMA$_{0.9}$)	80	20	22 767	125 063	5.493
DBIB-p(OEGMA$_{50}$)	100	0	15 020	18 700	1.245

^{a} TD-SEC using DMF/0.01 M LiBr eluent.
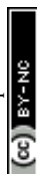
1.9 mL volumes of the HAuCl$_4$·3H$_2$O stock solution, aliquots of each polymeric solution were added at either 2 mL, 1 mL or 0.5 mL, with the total final volume subsequently adjusted to 20 mL by addition of deionised water. Thus, three concentrations for each were prepared containing 70 mg, 35 mg, and 17.5 mg of homo-polymer or (co)polymer.

The method ensured that final Au(III) concentration was consistently fixed at 0.5 mM throughout, equating to an Au(III) mass of 1.97 mg per sample. For simplicity, the approximate polymeric to Au(III) mass ratio (P : Au) may be represented as 35 : 1, 18 : 1 and 9 : 1. Identical solutions were prepared for both the linear and branched homo-polymers and (co)polymers, including the linear DBIB-p(OEGMA$_{50}$), synthesised through ATRP without MAA and avoiding the inclusion of thioether functionality. Therefore, at each polymeric concentration, there were five individual solutions prepared corresponding to the incremental increase in MAA contained in the polymeric structures: 0%, 5%, 10%, 15% and 20% MAA (Table 1). Additionally, a control was prepared where no polymer stabiliser was present and thus resultant AuNP colloidal stability was through anion charge stabilised (Cl$^-$ and BH$_4^-$) alone, resulting in a total of 34 solutions. To each solution under vigorous stirring, 2 mL of NaBH$_4$ (50 mM) was added. Upon addition, each solution turned from a pale yellow to a deep red colour indicating Au(III) reduction and gold particle formation. The solutions were left to stir for 24 hours before characterisation. Prior to analysis, the pH was measured for each solution and found to be approximately 8 across all AuNP mixtures. This is considerably above the typical MMA pK_a of $\sim$5,[50] thus suggesting the MAA groups to be in their negative, de-protonated form. AuNP diameters were calculated by monitoring the ratio of UV-vis absorption of the surface plasmon band (A_{spr}) at 520 nm with the absorption at 450 nm (A_{450}). This commonly employed methodology was developed by Haiss *et al.* to determine gold particle size, which shows that as particle sizes become smaller the A_{spr}/A_{450} ratio decreases.[49] This is clear in the UV-vis traces in Fig. 2, which show variation of A_{spr}/A_{450} with both differing polymeric concentrations and compositions, with the calculated size data in Table 2.

The first key observation is that no stable particle formation was observed when using DBIB-p(OEGMA$_{50}$); *i.e.* the homo-polymer containing neither thioether nor carboxylic acid groups; this was evident as sample colour (deep purple) and UV-vis spectra were not consistent with AuNP formation, suggesting particle aggregation. Conversely, for both DDT-p(OEGMA$_{50}$) and DDT-p(OEGMA$_{50}$-*co*-EGDMA$_{0.9}$), particle formation and stability occurred, *i.e.* when employing homo-polymer stabilisers bearing the thioether group but no carboxylic acid group. Therefore, homo-polymers containing OEGMA alone were not able to bind to the surface and stabilise AuNP formation and thus the importance of the thioether was highlighted.

In the presence of thioether containing branched and linear (co)polymers, AuNP particle sizes were consistently smaller than for the control samples generated in the absence of any polymeric stabiliser, *i.e.* charge stabilised by surface bound Cl$^-$ and BH$_4^-$ anions alone. Particle sizes were further made
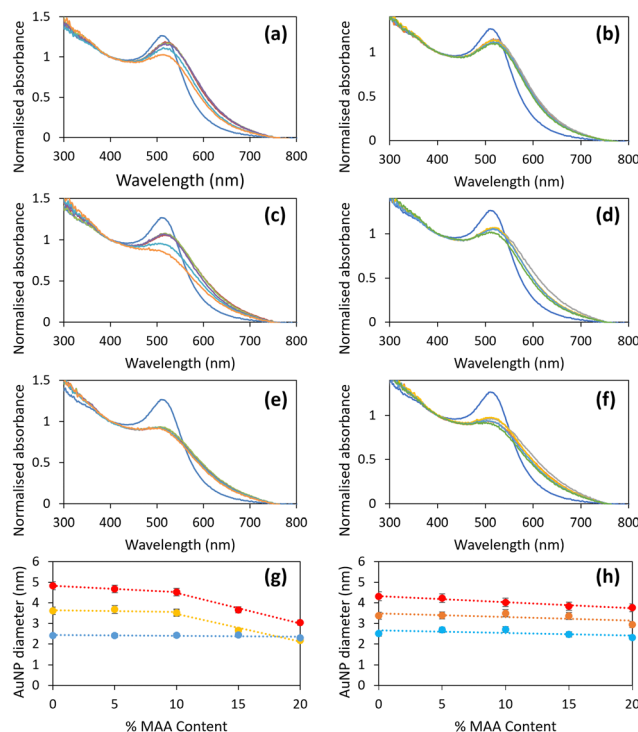

Fig. 2 UV-vis absorption traces for AuNPs prepared with polymeric stabilisers P : Au mass ratios at (a and b) 9 : 1, (c and d) 18 : 1 and (e and f) 35 : 1. Left (*i.e.* charts (a, c and e) show UV-vis traces for solutions prepared with liner polymeric structures; p(OEGMA$_x$-*co*-MAA$_y$); right (*i.e.* charts b, d and f) show UV-vis traces for solutions prepared with branched polymeric structures; p(OEGMA$_x$-*co*-MAA$_y$-*co*-EGDMA$_{0.9}$). Charts (a) to (f) show varying MAA : OEGMA x : y values as: 0 : 50 (dark blue); 2.5 : 47.5 (orange); 5 : 45 (grey); 7.5 : 42.5 (yellow); 10 : 40 (light blue). Calculated AuNP diameter *vs.* polymeric %MAA content are shown in charts (g) for linear and (h) for branched polymeric structures at 9 : 1 (red), 18 : 1 (yellow) and 35 : 1 (blue) P : Au mass ratios.

smaller as P : Au mass ratios were increased for both branched and linear (co)polymers until a minimum size of $\sim$2.3 nm was achieved, presumably because the AuNPs have reached the minimum size achievable under the synthetic conditions employed.

A significant observation with regards the linear (co)polymers was that the observed AuNP size growth was impeded as MAA content was increased (Fig. 2g and Table 2). At the lower P : Au mass ratios, smaller particle sizes were produced as (co)polymers containing a greater MAA component were used as stabiliser, which becomes more significant with MAA content at 15% and 20%. At the high P : Au mass ratio however, particle sizes were consistent irrespective of MAA content. In the presence of the branched equivalents, minor AuNP size reduction attributed to increasing MAA content was observed at all P:Au mass ratios, albeit much less than for the linear equivalents (Fig. 2h and Table 2).

Transmission electron spectroscopy (TEM) was employed for selected samples to image the particles formed. Samples were selected to represent the widest size ranges observed following UV-vis analysis. TEM analysis showed the same trend in AuNP particle size formation as observed *via* UV-vis spectroscopy (Fig. 3 and Table 2).

Table 2 AuNP sizes by diamater calculated by UV-vis absorption spectroscopy as well as AuNP hydrodynmic diameter (D_n) and surface zeta potential (ζ), determined by DLS and AuNP diameters as determined by TEM for each solution prepared using the library of (co)polymers as stabilisers

	P : Au	AuNP size UV (nm)	D_n (nm)	ζ (mV)
No stabilizer	n/a	5.61 ± 0.17	8.0	−18.7

Linear Homo-polymers and (co)polymers						Branched Homo-polymers and (co)polymers					
Structure	P : Au	AuNP size UV (nm)	AuNP size TEM (nm)	D_n (nm)	ζ (mV)	Structure	P : Au	AuNP size UV (nm)	AuNP size TEM (nm)	D_n (nm)	ζ (mV)
DDT-p(OEGMA$_{50}$)	9 : 1	4.83 ± 0.04	4.66 ± 0.87	17.7	−17.4	DDT-p(OEGMA$_{50}$-co-EGDMA$_{0.9}$)	9 : 1	4.31 ± 0.43	4.60 ± 1.15	17.9	−9.0
	18 : 1	3.61 ± 0.04	—	16.7	−17.0		18 : 1	3.37 ± 0.26	—	10.8	−8.6
	35 : 1	2.41 ± 0.08	3.02 ± 0.80	13.9	−16.2		35 : 1	2.51 ± 0.03	2.86 ± 0.81	9.4	−8.9
DDT-p(OEGMA$_{47.5}$-co-MAA$_{2.5}$)	9 : 1	4.68 ± 0.19	—	12.5	−25.7	DDT-p(OEGMA$_{47.5}$-co-MAA$_{2.5}$-co-EGDMA$_{0.9}$)	9 : 1	4.23 ± 0.35	—	11.4	−17.8
	18 : 1	3.68 ± 0.01	—	12.2	−32.4		18 : 1	3.38 ± 0.36	—	11.6	−19.7
	35 : 1	2.41 ± 0.06	—	11.8	−28.9		35 : 1	2.69 ± 0.09	—	9.4	−16.1
DDT-p(OEGMA$_{45}$-co-MAA$_5$)	9 : 1	4.53 ± 0.08	—	10.7	−21.7	DDT-p(OEGMA$_{45}$-co-MAA$_5$-co-EGDMA$_{0.9}$)	9 : 1	4.02 ± 0.50	—	13.0	−27.9
	18 : 1	3.52 ± 0.01	—	11.6	−34.5		18 : 1	3.49 ± 0.47	—	10.5	−25.7
	35 : 1	2.43 ± 0.06	—	9.6	−31.3		35 : 1	2.71 ± 0.42	—	10.9	−27.9
DDT-p(OEGMA$_{42.5}$-co-MAA$_{7.5}$)	9 : 1	3.66 ± 0.10	—	9.4	−34.8	DDT-p(OEGMA$_{42.5}$-co-MAA$_{7.5}$-co-EGDMA$_{0.9}$)	9 : 1	3.84 ± 0.45	—	9.8	−28.6
	18 : 1	2.67 ± 0.06	—	9.1	−42.4		18 : 1	3.36 ± 0.27	—	8.9	−28.0
	35 : 1	2.43 ± 0.04	—	11.6	−36.1		35 : 1	2.46 ± 0.11	—	10.5	−27.7
DDT-p(OEGMA$_{40}$-co-MAA$_{10}$)	9 : 1	3.04 ± 0.04	3.68 ± 0.82	8.5	−35.4	DDT-p(OEGMA$_{40}$-co-MAA$_{10}$-co-EGDMA$_{0.9}$)	9 : 1	3.77 ± 0.34	3.93 ± 1.26	10.8	−31.2
	18 : 1	2.17 ± 0.07	—	9.8	−41.3		18 : 1	2.95 ± 0.20	—	10.2	−29.3
	35 : 1	2.30 ± 0.04	3.11 ± 1.21	12.0	−41.3		35 : 1	2.32 ± 0.03	2.81 ± 0.69	10.2	−31.6

Surface zeta potentials (ζ) of each sample were also measured (Table 2); measurements were taken with samples as prepared to see the effect of displacement of surface bound BH_4^-. When DDT-p(OEGMA$_{50}$) was employed, ζ matched that of the control AuNP prepared in the absence of any stabiliser, while for DDT-p(OEGMA$_{50}$-co-EGDMA$_{0.9}$) ζ became more neutral, thus suggesting the branched homo-polymer displaced more surface bound BH_4^- than the linear equivalent. Upon introduction of MAA containing linear and branched (co)polymers, ζ generally became progressively more negative as MAA content increased, while the lower ζ values were observed for each branched (co)polymer *vs.* their linear analogue. The lower ζ values for the branched system would suggest that more of the acid groups are bound to the gold surface, while more acid groups remain free for the linear equivalents.

Hydrodynamic diameters (D_n) were observed to be similar between both linear and branched equivalents. In the cases of DBIB-p(OEGMA$_{50}$) and DDT-p(OEGMA$_{50}$-co-EGDMA$_{0.9}$), there is a general decrease in D_n upon increasing stabiliser concentration, which coincides with the large decrease with AuNP particle sizes observed by UV-vis spectroscopy. Conversely, as MAA is introduced to both branched and linear (co)polymers, the D_n values for the synthesised AuNPs remain relatively consistent despite the reduction in AuNP size observed by UV-vis, and in some cases slightly increased upon increasing concentration of stabiliser. Both the observed ζ and D_n data suggest architecture dependence on both stabiliser binding nature and an increase in the charge contribution to colloidal stability upon greater introduction of MAA.

The colloidal stability through either charge or steric stabilisation was investigated by addition of NaCl solution to each AuNP mixture. 200 µL aliquots of a 1 M NaCl solution were added to 1 mL of each AuNP dispersion. A total of six 200 µL aliquots were sequentially added to each AuNP dispersion, giving a final NaCl concentration of 0.55 M. After each addition,
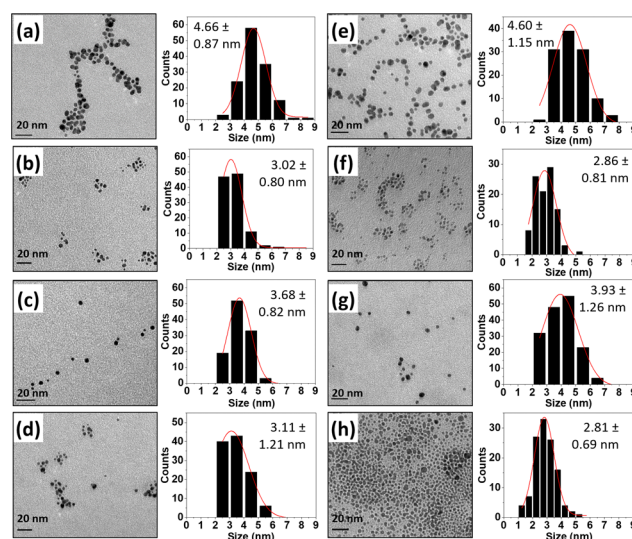

Fig. 3 TEM images of AuNPs prepared with polymeric stabilisers (a) DDT-p(OEGMA$_{50}$) at P : Au 9 : 1; (b) DDT-p(OEGMA$_{50}$) at P : Au 35 : 1; (c) DDT-p(OEGMA$_{40}$-co-MAA$_{10}$) at P : Au 9 : 1; (d) DDT-p(OEGMA$_{40}$-co-MAA$_{10}$) at P : Au 35 : 1; (e) DDT-p(OEGMA$_{50}$-co-EGDMA$_{0.9}$) at P : Au 9 : 1; (f) DDT-p(OEGMA$_{50}$-co-EGDMA$_{0.9}$) at P : Au 35 : 1; (g) DDT-p(OEGMA$_{40}$-co-MAA$_{10}$-co-EGDMA$_{0.9}$) at P : Au 9 : 1; (h) DDT-p(OEGMA$_{40}$-co-MAA$_{10}$-co-EGDMA$_{0.9}$) at P : Au 35 : 1. Hystograms show particle size distribution analysis, generated through measurement of over 100 AuNPs for the statistical analysis.

samples were analysed by UV-vis spectroscopy to monitor changes in AuNP size, and once the titration was complete, the ζ values were recorded. Upon addition of the NaCl first aliquot to the control AuNP prepared in the absence of polymeric stabiliser, immediate aggregation and precipitation occurred, with the solution colour changing from red to dark purple. Colloidal stability, however, was maintained for all

polymeric stabilised AuNP solutions throughout the titration with no variation in observed AuNP size. ζ values showed neutralisation of charge upon salt addition, thus suggesting steric stabilisation *via* OEGMA to dominate (see Fig. S12 and S13 (ESI†) for titration plots and solution images post salt addition).

Catalytic reduction of 4-nitrophenol to 4-aminophenol

The variation in polymeric architecture and gold particle surface binding may result in differing catalytic behaviour of the prepared AuNPs. In order to explore this, studies of the use of the AuNPs as catalysts for the reduction of 4-NP by NaBH$_4$ were conducted. Wunder *et al.* proposed the Langmuir–Hinshelwood mechanistic model for the catalytic reduction process in which BH$_4^-$ binds and 4-NP adsorbs onto the gold particle surface where the reduction of 4-NP to 4-AP occurs.[51,52] It is necessary for both BH$_4^-$ ions and 4-NP to be present on the AuNP surface concomitantly in order for the reduction to take place (Fig. 4). Ciganda *et al.*, demonstrated that the surface restructuring through stabilising ligand displacement by the reactive substrates to be a key feature in the Langmuir–Hinshelwood mechanism.[53] An induction time arises as ligand displacement and surface restructuring occurs prior to catalytic reduction; stronger surface binding ligand stabilisers will render surface rearrangement more difficult, thus induction times will be longer than for stabilising ligands with comparatively weaker surface binding affinity. More recently, Gao *et al.* demonstrated a reduction in catalytic activity upon increased steric hindrance around the AuNP surface. They showed that upon increasing the carbon chain length of surface stabilising ligands through the use and comparison of 3-mercaptopropionic acid (MPA) verses 1-mercaptoundecanoic acid (MUA), the observed apparent rate constants of the catalytic reduction of 4-NP were decreased.[54]

It was thus hypothesised that the alteration of the polymeric stabilisers employed herein may result in variation of: (a) induction times through variation in the nature of the surface ligand binding, *i.e.* weaker MAA carboxylic acid group surface binding *c.f.* stronger thioether surface binding; (b) overall apparent rate constants through variation of steric hindrance through different polymeric architectures. The catalytic

Fig. 4 Schematic of the catalytic reduction of 4-nitrophenol (4-NP) to 4-aminophenol (4-AP) by NaBH$_4$ showing the Langmuir–Hinshelwood mechanistic model.

reaction was monitored by UV-vis spectroscopy. Upon addition of 4-NP to gold particle catalysts in the presence of NaBH$_4$, there is an observed decrease in the 4-NP absorption band at $\sim$400 nm, and the emergence of the less intense 4-AP and at $\sim$300 nm. In order to ensure first order rate kinetics with respect to 4-NP, an excess of NaBH$_4$ is used. Thus, the integrated rate law can be applied to calculate the apparent first order rate constant, k_{app} through eqn (1):

$$-\ln(A_t/A_o) = k_{app}t \qquad (1)$$

where t = time (seconds), A_o = initial absorbance of 4-NP and A_t is the absorbance of 4-NP at time t. The decrease of the 4-NP band is observed only after the induction time (t_i) has passed. Thus, A_o remains constant for the duration of t_i, with the apparent rate constant determined from the gradient of the $-\ln(A_o/A_t)$ *vs.* t plot following the induction time period. To illustrate this, Fig. 5 shows the observed fastest (DDT-p(OEGMA$_{40}$-*co*-MAA$_{10}$-*co*-EGDMA$_{0.9}$) at 9:1 P:Au mass ratio) and slowest DDT-p(OEGMA$_{50}$) at 35:1 P:Au) observed 4-NP reduction reactions. Fig. 6 shows a chart of all the calculated apparent rate constants across AuNPs prepared at all polymeric concentrations (see Fig. S14–S23 and Table S1 (ESI†) for full UV-vis absorption data for catalytic monitoring). It is evident that upon increased P:Au ratio, the rate of reaction was decreased while induction times increased. This would be expected as increased ligand surface packing density would reduce gold surface accessibility to the reactive species, while greater ligand rearrangement would be required upon increased stabiliser concentrations.[55] A significant observation is that at fixed (co)polymer concentrations, and increasing MAA content per (co)polymer, the rate of reaction increased almost linearly, while induction times decreased. Secondly, branched (co)polymer stabilised AuNPs demonstrated faster rate constants than their linear equivalents, with an observed reduction in induction time at the lower MAA content percentage (0–5% MAA) with similar or slightly longer induction times at the higher MAA content percentage (10–20% MAA). It is clear, therefore, that (co)polymer composition and architecture influenced the catalytic activity of the AuNPs.

Upon increased MAA content for both branched and linear polymeric stabilisers, the rates of reaction increased while induction times decreased. Thus, it can be concluded that the introduction of MAA allows for more facile substrate access to the AuNP surface, with greater ease of surface restructuring. Secondly, In the case of the branched polymeric stabilisers, there is an increase in the rate of catalytic reaction for all with respect to their linear analogues, thus it can be further be concluded that the effect of increased MAA content is greater for the branched stabilisers than their linear equivalents.

Poly(OEGMA) has a polymer-brush architecture. As such, it is hypothesised that as MAA is introduced, the polymer becomes less "brush-like" and allows for MAA to reversibly bind and release from the AuNP surface forming small polymer loops on the AuNP surface. As (co)polymers baring a greater MAA content are introduced, greater reversible MAA binding occurs. This would allow for easier substrate access to the AuNP
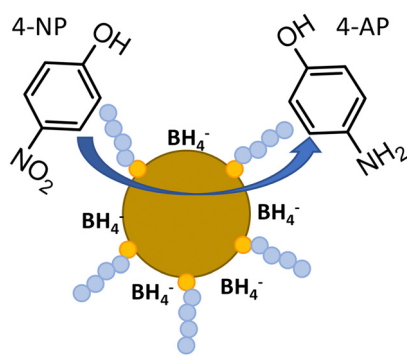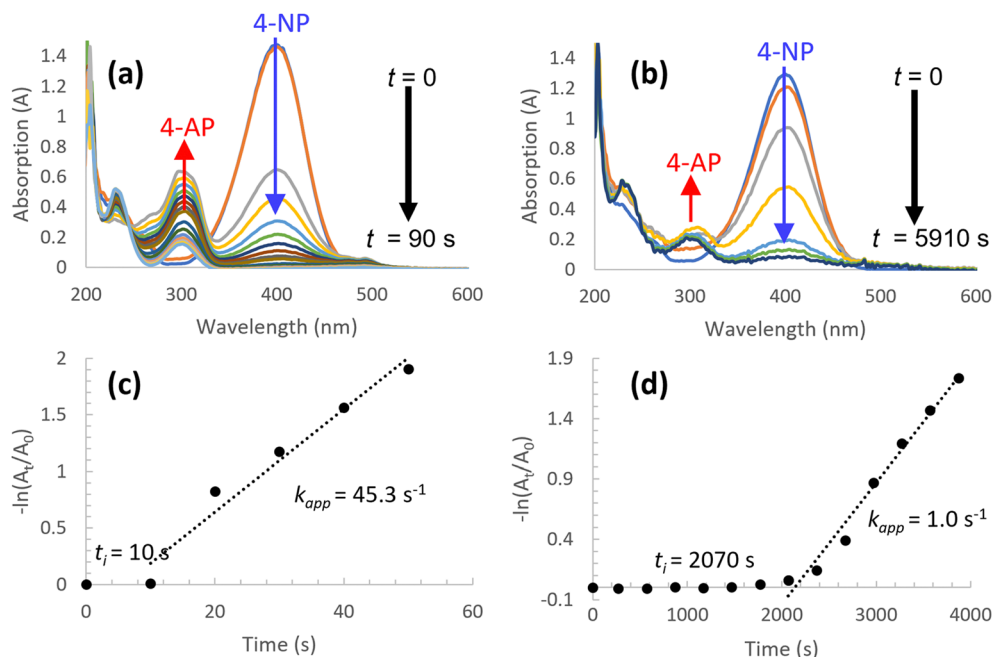
Fig. 5 Catalytic reduction of 4-NP to 4-AP. Above show UV-vis absorption traces, and below show −ln(A_t/A_o) *vs.* *t* plots used to determine apparent rate constant (k_{app}) and induction times (t_i) for AuNP samples prepared with (a and c) DDT-*p*(OEGMA$_{40}$-*co*-MAA$_{10}$-*co*-EGDMA$_{0.9}$) at 9 : 1 P : Au mass ratio, and (b and d) DDT-*p*(OEGMA$_{50}$) at 35 : 1 P : Au mass ratios (see Fig. S14–S23 and Table S1 (ESI†) for full UV-vis absorption data for catalytic monitoring of all samples).
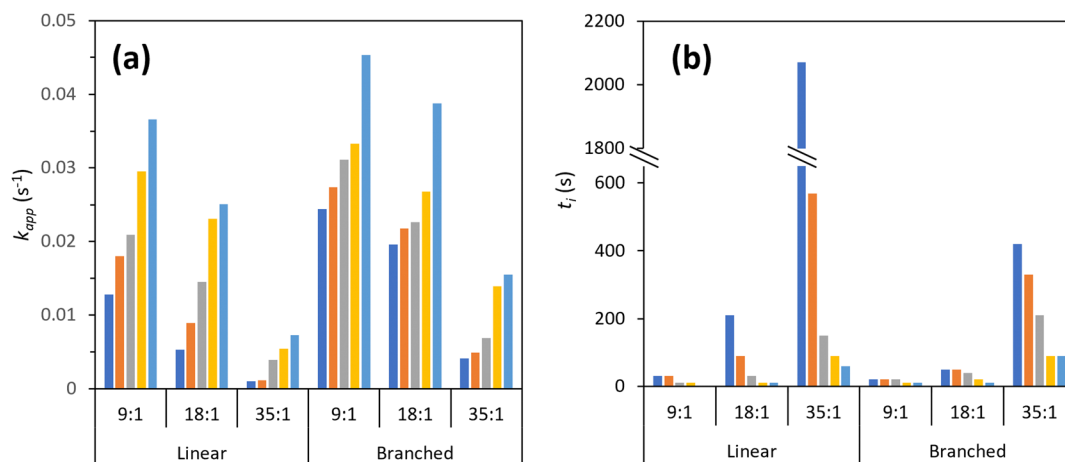

Fig. 6 Catalytic reduction of 4-NP to 4-AP, determined by UV-vis spectroscopy, showing (a) comparative apparent rate constants (k_{app}) and (b) induction times (t_i) for AuNP solutions prepared using the library of linear and branched polymeric stabilisers at 9 : 1, 18 : 1 and 35 : 1 P : Au mass ratios. Dark blue bars: DDT-*p*(OEGMA$_{50}$) or DDT-*p*(OEGMA50-*co*-EGDMA$_{0.9}$); orange bars: DDT-*p*(OEGMA$_{47.5}$-*co*-MAA$_{2.5}$) or DDT-*p*(OEGMA$_{47.5}$-*co*-MAA$_{2.5}$-*co*-EGDMA$_{0.9}$); grey bars; DDT-*p*(OEGMA$_{45}$-*co*-MAA$_5$) or DDT-*p*(OEGMA$_{45}$-*co*-MAA$_5$-*co*-EGDMA$_{0.9}$); yellow bars: DDT-*p*(OEGMA$_{42.5}$-*co*-MAA$_{7.5}$) or DDT-*p*(OEGMA$_{42.5}$-*co*-MAA$_{7.5}$-*co*-EGDMA$_{0.9}$); light blue bars; DDT-*p*(OEGMA$_{40}$-*co*-MAA$_{10}$) or DDT-*p*(OEGMA$_{40}$-*co*-MAA10-*co*-EGDMA$_{0.9}$).

surface and shorter surface rearrangement times as ligand surface biding becomes more dynamic, which accounts for the faster kinetics and reduced reduction times observed during the catalytic studies. This hypothesis is suggested for both linear and branched polymeric structures. The similar D_n values between linear and branched analogues (Table 2) suggest similar surface stabilisation nature where a hybrid model of polymer loops through MAA and dangling chains of OEGMA

form, resulting in comparable hydrodynamic diameters. It is suggested, therefore, that architectural difference between linear and branched analogues gives rise to a greater and more rapid degree of reversible MAA polymer loop formation for the branched polymeric stabilisers than for their linear equivalents, resulting in the observed increased catalytic rate and reduced induction times observed during the catalytic studies.

Conclusions

The hypothesis draws on the observations made during this study, which demonstrate that variation in both (co)polymer composition, architecture, and concentration do impact the size properties within the range of 2–5 nm when used as stabilisers for the synthesis of AuNPs. The catalytic reduction of 4-NP to 4-AP demonstrated around a 45-fold variability in reaction rates and a 2000-fold variation in induction times, dictated by polymeric composition, architecture and concentration effects on AuNP surface chemistry. Herein, the study focused on polymer composition and architecture, however future studies investigating polymer response to stimuli would also be of considerable interest, e.g. when solvent change, temperature or pH are applied. With further investigation, this could be exploited and applied to alternate polymeric systems and AuNP catalytic reactions and uses to fine tune generation of AuNPs with both specific size properties and surface chemistry behaviour.

Author contributions

DT, SR and MG designed the experiments and wrote the manuscript. DT, JH, EC and SE optimised the experimental conditions for polymer synthesis. DT prepared all AuNP solutions and ran all UV-vis, DLS and zeta potential analysis. EUH carried out TEM measurements. All authors contributed towards editing of the manuscript.

Conflicts of interest

There are no conflicts to declare.

Acknowledgements

References

1 H. Chen, X. Kou, Z. Yang, W. Ni and J. Wang, *Langmuir*, 2008, **24**, 5233–5237.

2 M. C. Daniel and D. Astruc, *Chem. Rev.*, 2004, **104**, 293–346.

3 E. C. Dreaden, A. M. Alkilany, X. Huang, C. J. Murphy and M. A. El-Sayed, *Chem. Soc. Rev.*, 2012, **41**, 2740–2779.

4 E. Boisselier and D. Astruc, *Chem. Soc. Rev.*, 2009, **38**, 1759–1782.

5 K. Saha, S. S. Agasti, C. Kim, X. Li and V. M. Rotello, *Chem. Rev.*, 2012, **112**, 2739–2779.

6 P. D. Howes, R. Chandrawati and M. M. Stevens, *Science*, 2014, **346**, 53.

7 J. N. Anker, W. P. Hall, O. Lyandres, N. C. Shah, J. Zhao and R. P. Van Duyne, *Nat. Mater.*, 2009, **7**, 442–453.

8 J.-F. Masson, *ACS Sens.*, 2017, **2**, 16–30.

9 In *Localized Surface Plasmon Resonance Based Nanobiosensors*, ed. Y.-T. Long and C. Jing, 2014, Springer International Publishing.

10 M. U. Farooq, V. Novosad, E. A. Rozhkova, H. Wali, A. Ali, A. A. Fateh, P. B. Neogi, A. Neogi and Z. Wang, *Sci. Rep.*, 2018, **8**, 1–12.

11 P. Ghosh, G. Han, M. De, C. K. Kim and V. M. Rotello, *Adv. Drug Delivery Rev.*, 2008, **60**, 1307–1315.

12 J. B. Vines, J. H. Yoon, N. E. Ryu, D. J. Lim and H. Park, *Front. Chem.*, 2019, **7**, 1–16.

13 A. M. Lopatynskyi, Y. O. Malymon, V. K. Lytvyn, I. V. Mogylnyi, A. E. Rachkov, A. P. Soldatkin and V. I. Chegel, *Plasmonics*, 2018, **13**, 1659–1669.

14 S. Huo, S. Jin, X. Ma, X. Xue, K. Yang, A. Kumar, P. C. Wang, J. Zhang, Z. Hu and X. J. Liang, *ACS Nano*, 2014, **8**, 5852–5862.

15 E. R. Figueroa, A. Y. Lin, J. Yan, L. Luo, A. E. Foster and R. A. Drezek, *Biomaterials*, 2014, **35**, 1725–1734.

16 S. Her, D. A. Jaffray and C. Allen, *Adv. Drug Delivery Rev.*, 2017, **109**, 84–101.

17 K. Haume, S. Rosa, S. Grellet, M. A. Śmiałek, K. T. Butterworth, A. V. Solov'yov, K. M. Prise, J. Golding and N. J. Mason, *Cancer Nanotechnol.*, 2016, **7**, 1–20.

18 A. A. Borran, A. Aghanejad, A. Farajollahi, J. Barar and Y. Omidi, *Radiat. Phys. Chem.*, 2018, **152**, 137–144.

19 B. Reiser, L. González-García, I. Kanelidis, J. H. M. Maurer and T. Kraus, *Chem. Sci.*, 2016, **7**, 4190–4196.

20 D. Juric, H. Hao, E. Ermantraut, K. Glaser, W. Eberhardt and A. Zimmermann, *IEEE Trans. Compon. Packag. Technol.*, 2020, **10**, 325–331.

21 R. C. Zhang, D. Sun, R. Zhang, W. F. Lin, M. Macias-Montero, J. Patel, S. Askari, C. McDonald, D. Mariotti and P. Maguire, *Sci. Rep.*, 2017, **7**, 1–9.

22 T. Mitsudome and K. Kaneda, *Green Chem.*, 2013, **15**, 2636–2654.

23 B. S. Takale, M. Bao and Y. Yamamoto, *Org. Biomol. Chem.*, 2014, **12**, 2005–2027.

24 P. Suchomel, L. Kvitek, R. Prucek, A. Panacek, A. Halder, S. Vajda and R. Zboril, *Sci. Rep.*, 2018, **8**, 1–11.

25 S. Wang, J. Wang, Q. Zhao, D. Li, J. Q. Wang, M. Cho, H. Cho, O. Terasaki, S. Chen and Y. Wan, *ACS Catal.*, 2015, **5**, 797–802.

26 A. Gangula, R. Podila, R. M, L. Karanam, C. Janardhana and A. M. Rao, *Langmuir*, 2011, **27**, 15268–15274.

27 Y. S. Seo, E. Y. Ahn, J. Park, T. Y. Kim, J. E. Hong, K. Kim, Y. Park and Y. Park, *Nanoscale Res. Lett.*, 2017, **12**, 1–11.

28 C. Deraedt, L. Salmon, S. Gatard, R. Ciganda, R. Hernandez, M. Mayor and D. Astruc, *Chem. Commun.*, 2014, **50**, 14194–14196.

29 S. Noël, H. Bricout, A. Addad, C. Sonnendecker, W. Zimmermann, E. Monflier and B. Léger, *New J. Chem.*, 2020, **44**, 21007–21011.

30 M. Grzelczak, J. Pérez-Juste, P. Mulvaney and L. M. Liz-Marzán, *Chem. Soc. Rev.*, 2008, **37**, 1783–1791.

31 J. Turkevich, P. C. Stevenson and J. Hiller, *Discuss. Faraday Soc.*, 1951, **11**, 55–75.

32 G. Frens, *Nat. Phys. Sci.*, 1973, **241**, 20–22.

33 M. Brust, M. Walker, D. Bethell, D. J. Schiffrin and R. Whyman, *J. Chem. Soc., Chem. Commun.*, 1994, 801–802.

34 S. R. K. Perala and S. Kumar, *Langmuir*, 2013, **29**, 9863–9873.

35 L. M. Liz-Marzán, *Chem. Commun.*, 2013, **49**, 16–18.

36 In *Noble Metal Nanoparticles: Preparation, Composite Nanostructures, Biodecoration and Collective Properties*, ed. I. Capek, 2014, Springer International Publishing.

37 In *Gold Clusters, Colloids and Nanoparticles I*, ed. D. -M. P. Mingos, 2014, Springer International Publishing.

38 K. R. Brown, D. G. Walter and M. J. Natan, *Chem. Mater.*, 2000, **12**, 306–313.

39 J. Kimling, M. Maier, B. Okenve, V. Kotaidis, H. Ballot and A. Plech, *J. Phys. Chem. B*, 2006, **110**, 15700–15707.

40 J. Manson, D. Kumar, B. J. Meenan and D. Dixon, *Gold Bull.*, 2011, **44**, 99–105.

41 H. Kang, J. T. Buchman, R. S. Rodriguez, H. L. Ring, J. He, K. C. Bantz and C. L. Haynes, *Chem. Rev.*, 2019, **119**, 664–699.

42 Y. Dai and X. Zhang, *Macromol. Mater. Eng.*, 2018, **303**, 1–8.

43 F. Masse, P. Desjardins, M. Ouellette, C. Couture, M. M. Omar, V. Pernet, S. Guérin and E. Boisselier, *Molecules*, 2019, **24**, 15–17.

44 K. Rahme, L. Chen, R. G. Hobbs, M. A. Morris, C. O'Driscoll and J. D. Holmes, *RSC Adv.*, 2013, **3**, 6085–6094.

45 J. V. Jokerst, T. Lobovkina, R. N. Zare and S. S. Gambhir, *Nanomedicine*, 2011, **6**, 715–728.

46 I. Hussain, S. Graham, Z. Wang, B. Tan, D. C. Sherrington, S. P. Rannard, A. I. Cooper and M. Brust, *J. Am. Chem. Soc.*, 2005, **127**, 16398–16399.

47 Z. Wang, B. Tan, I. Hussain, N. Schaeffer, M. F. Wyatt, M. Brust and A. I. Cooper, *Langmuir*, 2007, **23**, 885–895.

48 S. E. Edwards, S. Flynn, J. J. Hobson, P. Chambon, H. Cauldbeck and S. P. Rannard, *RSC Adv.*, 2020, **10**, 30463–30475.

49 W. Haiss, N. T. K. Thanh, J. Aveyard and D. G. Fernig, *Anal. Chem.*, 2007, **79**, 4215–4221.

50 E. L. Ibarra-Montaño, N. Rodríguez-Laguna, A. Sánchez-Hernández and A. Rojas-Hernández, *J. Appl. Sol. Chem. Model.*, 2015, **4**, 7–18.

51 S. Wunder, F. Polzer, Y. Lu, Y. Mei and M. Ballauff, *J. Phys. Chem. C*, 2010, **114**, 8814–8820.

52 S. Wunder, Y. Lu, M. Albrecht and M. Ballauff, *ACS Catal.*, 2011, **1**, 908–916.

53 R. Ciganda, N. Li, C. Deraedt, S. Gatard, P. Zhao, L. Salmon, R. Hernández, J. Ruiz and D. Astruc, *Chem. Commun.*, 2014, **50**, 10126–10129.

54 M. Gao, Y. Yang and J. Guo, *Catal. Lett.*, 2019, **149**, 2110–2118.

55 S. M. Ansar and C. L. Kitchens, *ACS Catal.*, 2016, **6**, 5553–5560.